

Star formation histories of early-type galaxies at $z = 1.2$ in cluster \star and field $\star\star$ environments

R. Gobat¹, P. Rosati¹, V. Strazzullo^{1,2}, A. Rettura³, R. Demarco³, and M. Nonino⁴

¹ European Southern Observatory, Karl Schwarzschild Strasse 2, Garching bei Muenchen, D-85748, Germany

² National Radio Astronomy Observatory, P.O. Box O, Socorro, NM, 87801, USA

³ Department of Physics and Astronomy, Johns Hopkins University, Baltimore, MD21218. USA

⁴ INAF-Osservatorio Astronomico di Trieste, via G.B. Tiepolo 11, 34131 Trieste, Italy

Received 7 February 2008; accepted 26 June 2008

ABSTRACT

We derive the star formation histories of early-type galaxies at $z \simeq 1.2$ in both low and high density environments. To this purpose, we compare the co-added spectroscopic and 8-9 band photometric data of 43 mass selected early-type galaxies in the massive cluster RDCS J1252.9-2927 and the GOODS/CDF-S field with a large grid of composite stellar population models based on the Bruzual & Charlot templates. We find that the cluster early-type galaxies formed the bulk of their stars approximately 0.5 Gyr earlier than early-types in the field, whereas field early-types presumably finish forming their stellar content on a longer time scale. Such a difference is particularly evident at masses $\lesssim 10^{11} M_{\odot}$, whereas it becomes negligible for the most massive galaxies. While our differential analysis of the stellar population parameters of cluster and field galaxies in the same mass range convincingly shows distinct star formation histories, the absolute age difference remains model dependent. Using the star formation histories that best fit the SEDs of the red sequence galaxies in RDCS 1252.9-2927, we reconstruct the evolution of the cluster red sequence and find that it was established over 1 Gyr and is expected to dissolve by $z \approx 2$.

Key words. galaxies:clusters:individual:RDCS 1252.9-2927 – galaxies:evolution – galaxies:elliptical

1. Introduction

Massive early-type galaxies are a good tracer of the early mass assembly in the Universe. The study of their spectrophotometric and morphological properties, especially at high redshift, over a range of environmental densities, can significantly constrain the different models of structure formation: the monolithic collapse (e.g. Eggen et al. 1962), in which early-type galaxies result from a single burst of star formation at high redshift, and the hierarchical model (e.g. Toomre 1977), where they form by the merger of low mass progenitors. This latter process is naturally expected in a Λ CDM cosmology and predicts different formation histories whether a galaxy is in a low-density environment or the member of a cluster (e.g. De Lucia et al. 2006). Indeed, the analysis of the fossil record via line-strength indices shows that massive early-type galaxies in local high-density environments are at least 1.5 Gyr older than their counterparts in low-density regions (Thomas et al. 2005, Sánchez-Blázquez et al. 2006, Clemens et al. 2006), while from the mass-to-light ratio of cluster and field galaxies up to $z \sim 1$, van Dokkum & van der Marel (2007) find a lower value of ~ 0.4 Gyr. On the other hand, early-type galaxies appear to have formed at an early time and been in place at $z \simeq 2$ (Bernardi et al. 1998, van Dokkum et al. 2001), with little star formation happening ever since. This suggests that studying the star formation history of early-type galaxies at $z > 1$ allows one to place stronger constraints on structure formation models than at low redshift, where any difference has been smoothed out by billions of years of mostly passive evolution and occasional mergers. In such a case, much sparser data are available, as few massive galaxy clusters have been observed so far at $z > 1$. One of these, RDCS J1252.9-2927 (Rosati et al. 2004) at $z = 1.24$, has had an extensive multi-wavelength spectroscopic coverage. In this paper, we use the spectrophotometric data of early-type galaxies in RDCS J1252.9-2927 to reconstruct their general star formation history and compare it with early-type galaxies from the GOODS/CDF-S at similar redshift. An independent analysis of the same data sets, also including morphological properties and far-UV rest-frame photometry is presented in Rettura et al. (2008). This paper is structured as follows. In Sect. 2, we describe our data and sample selection; in Sect. 3 we present our methodology and in Sect. 4 we describe and discuss the results of our analysis. We assume a Λ CDM cosmology with $\Omega_m = 0.3$, $\Omega_{\Lambda} = 0.7$ and $H_0 = 70 \text{ km s}^{-1} \text{ Mpc}^{-1}$. All magnitudes in this paper are given in the AB system (Oke 1974), unless stated otherwise.

* Based on observations carried out using the ESO VLT under Program IDs 166.A-0701, 69.A-0683, 73.A-0832 and 76.A-0889
** Observations have been carried out using the Very Large Telescope at the ESO Paranal Observatory under Program IDs 170.A-0788, 074.A-0709 and 275.A-5060

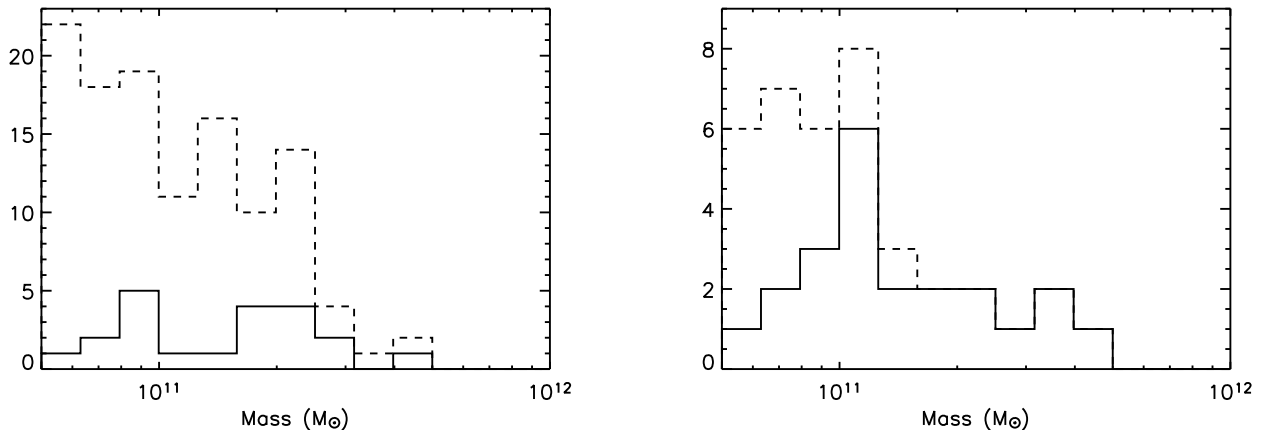


Fig. 1. Number of galaxies in the GOODS (*left*) and RDCS 1252 (*right*) samples as a function of the photometric stellar mass. The dashed line shows the photometric sample and the solid line the spectroscopic sample.

2. Data and sample selection

This work is based on photometric and spectroscopic data from the GOODS/CDF-S (hereafter GOODS, Giavalisco et al. 2004) field and the field around the cluster RDCS J1252.9-2927 (hereafter RDCS 1252; Rosati et al. 2004) at $z = 1.237$ (Demarco et al. 2007).

The data for the GOODS field comprises observations in 8 bands in the 0.4-5 μm range, namely the F435W, F606W, F775W and F850LP (hereafter b_{435} , v_{606} , i_{775} and z_{850} respectively) passbands with *HST*/ACS, the J and K_s bands with *VLT*/ISAAC (Retzlaff et al., in prep.) and at 3.6 and 4.5 μm with *Spitzer*/IRAC. In addition, we use spectra taken using *VLT*/FORS2 with the 300I grism, which provides a resolution of about 13\AA at 8600\AA (Vanzella et al. 2006, 2008).

For RDCS 1252, we used imaging in the B, V and R bands with *VLT*/FORS2, i_{775} and z_{850} with *HST*/ACS (Blakeslee et al. 2003), J_s and K_s with *VLT*/ISAAC (Lidman et al. 2004) and at 3.6 and 4.5 μm with *Spitzer*/IRAC. An extensive spectroscopic campaign of this cluster was carried out with *VLT*/FORS2 using the 300I grism (Demarco et al. 2007).

As a result, the two datasets used in our analysis have similar quality and wavelength coverage, thus yielding homogeneous spectrophotometric properties of galaxies and allowing a single selection criterion for both samples. Specifically, the availability of 8 to 9 passbands allows the estimate of reliable photometric stellar masses (Rettura et al. 2006). This work is based on two samples of early-type galaxies with available spectroscopy and covering the same mass range. One is extracted from the cluster spectroscopic sample and compared with a field sample drawn from the GOODS spectroscopic survey of galaxies in a small redshift bin around the cluster redshift. For all galaxies we have photometric stellar masses derived by SED fitting with composite stellar population models (Rettura et al. 2006). These were computed assuming solar metallicity and a Salpeter (1955) initial mass function, using the Bruzual & Charlot (2003, hereafter BC03) code.

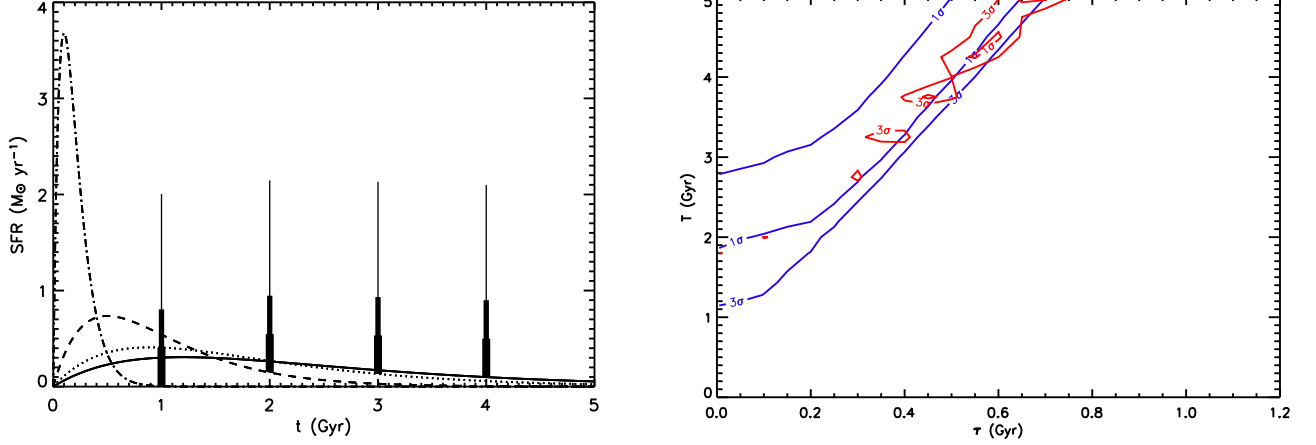
The near-IR depth of both samples allows us to define complete mass-selected samples. The GOODS and RDCS 1252 K_s -band images are photometrically complete down to $K_s = 24$. At $z \simeq 1.2$, the K_s -band photometry is a very good proxy of the stellar mass (Gavazzi et al. 1996), with $10^{10} M_\odot$ corresponding to $K_s \simeq 23$ (Strazzullo et al. 2006), which we take as a reliable mass completeness limit. On the other hand, the spectroscopic follow-up work is limited to $K_s \simeq 22$ for early-type galaxies in both samples, corresponding to $R_{Vega} \simeq 25$ and $M_\star \simeq 3 \times 10^{10} M_\odot$. Therefore, we limit our analysis to photometric stellar masses greater than $M_{lim} = 5 \times 10^{10} M_\odot$.

The selection of early-type galaxies in the cluster is apparent from the well-defined red sequence (Blakeslee et al. 2003) which clearly lies above $i_{775} - z_{850} = 0.8$, which thus separates the population of blue star-forming galaxies at the cluster redshift. We have spectra for 22 of the 38 galaxies on the red sequence with $M_\star \geq M_{lim}$. For the corresponding GOODS field sample, we select galaxies with $M_\star \geq M_{lim}$, in the redshift range $z = 1.237 \pm 0.15$ and adopt the same $i_{775} - z_{850} \geq 0.8$ cut used in RDCS 1252. This criterion yields 21 early-type galaxies with FORS2 spectra. We verify that the spectra do not show signs of ongoing star formation, i.e. that no [OII] $\lambda 3727$ emission line is detectable (we assume that the galaxies in our samples are dust-free; see Rettura et al. (2006)). We note that the vast majority of the galaxies in both samples have E/S0 morphologies following the classification scheme used by Blakeslee et al. (2003). Of the 18 galaxies in our GOODS sample found in the GEMS catalog (Häussler et al. 2007), all have $n \geq 3$.

An important aspect to be addressed is the relative spectroscopic completeness as a function of mass of the GOODS and RDCS 1252 samples, which should be considered when interpreting the results from our comparative spectrophotometric analysis. This can be quantified with accurate photometric redshifts available for our samples, which were derived using the Coleman et al. (1980) templates and the BPZ code (Benítez 2000), as described in Toft et al. (2004). Using photometric redshifts, we find 117 GOODS galaxies in the given redshift bin, with $i_{775} - z_{850} \geq 0.8$ and $M_\star \geq M_{lim}$.

In Fig. 1, we compare the photometric mass distributions of our color- and mass-selected galaxies in GOODS and RDCS 1252 to the mass distribution of the spectroscopically observed subsamples. It is immediately apparent that the spectroscopic follow-up work was more extensive in RDCS 1252 than in GOODS; as a result the GOODS spectroscopic

sample	Lower mass cutoff ($\times 10^{10} M_{\odot}$)			
	5	9	15	23
GOODS	18%	25%	35%	67%
RDCS 1252	59%	83%	100%	100%

Table 1. Cumulative spectroscopic completeness of the GOODS and RDCS 1252 samples.**Fig. 2.** *Left panel:* range of star formation histories spanned by the grid of BC models (the secondary bursts are not to scale with respect to the delayed exponential). *Right panel:* confidence contours (1σ and 3σ) obtained by fitting the co-added photometry (blue) and spectroscopic data (red) from the GOODS sample with a delayed exponential SFH without secondary burst.

sample is more incomplete at the low mass end than the RDCS 1252 sample (table 1). We will return to this point when discussing our results.

3. Spectrophotometric fitting method

We compare our spectrophotometric data to composite stellar population (CSP) synthesis models generated with the GALAXEV population synthesis code (Bruzual & Charlot 2003) using a χ^2 goodness-of-fit test. We choose the BC03 models for their high-resolution templates which allow us to fit both broad-band photometry and spectra. Because of the low signal-to-noise ratio of the available FORS2 spectra (ranging from 5 to 6 at 8000 \AA), we resort to stacking spectra of galaxies within the aforementioned stellar mass range separately for our cluster and field samples. Consequently, the photometric points are also co-added in the combined fit. We assume a delayed exponential star formation history (SFH), which is similar to the one proposed by Sandage (1986) and is more realistic than a simple exponentially declining SFH (Gavazzi et al. 2002), parametrized by a time-scale τ . Since we use both broad-band SEDs and spectroscopic features, we allow for more complex star formation histories. We expand the grid of models by adding secondary episodes of star formation after the main event parametrized by an instantaneous burst at time $t_{burst} > \tau$ of amplitude A , so that the star formation rate is expressed as :

$$\Psi(t) = \tau^{-2} t e^{-\frac{t}{\tau}} + A \delta(t - t_{burst}). \quad (1)$$

We consider age values, i.e. the time T after the onset of star formation, ranging from 200 Myr to 5 Gyr in increments of ~ 250 Myr. The time-scale τ ranges from 0 (corresponding to a simple stellar population) to 1 Gyr in increments of 0.1 Gyr. In the case of a secondary burst, t_{burst} ranges from 1 to 4 Gyr in increments of 1 Gyr with amplitudes A of 0.1, 0.2 and 0.5, which correspond to $1/11$, $1/6$ and $1/3$ of the final stellar mass respectively. Thus, the grid $\{T, \tau, t_{burst}, A\}$ contains $20 \times 13 \times 4 \times 3 + 13 \times 20 = 3380$ models. All models are computed at solar metallicity and are dust-free. We will comment on this assumption later. In Fig. 2, left, we show a sample of our grid of star formation histories.

We first use this grid of models to fit the stacked SEDs, covering rest-frame wavelengths from 2000 \AA to $2 \mu\text{m}$, which gives us a sub-grid of acceptable models within the confidence interval defined by $\chi^2 \leq \chi_0^2 + 16.25$ (where χ_0^2 is the minimum χ^2 solution) which corresponds to 3σ for the 5 fitting parameters: age, τ , t_{burst} , A and stellar mass. Among this subsample of models, we select those which best fit the stacked spectral data, adopting the same 3σ confidence level. These solutions will be referred to as the “best fit models” in the following.

In Fig. 2, right, we show the projection of the 3σ confidence levels of the fit on the stacked SEDs and spectra of the GOODS sample in the $\{T, \tau, t_{burst} = 0(\text{no burst}), A = 0\}$ plane. In Fig. 3, we show the SEDs and spectra of the best fitting models, with the stacked spectrophotometric data.

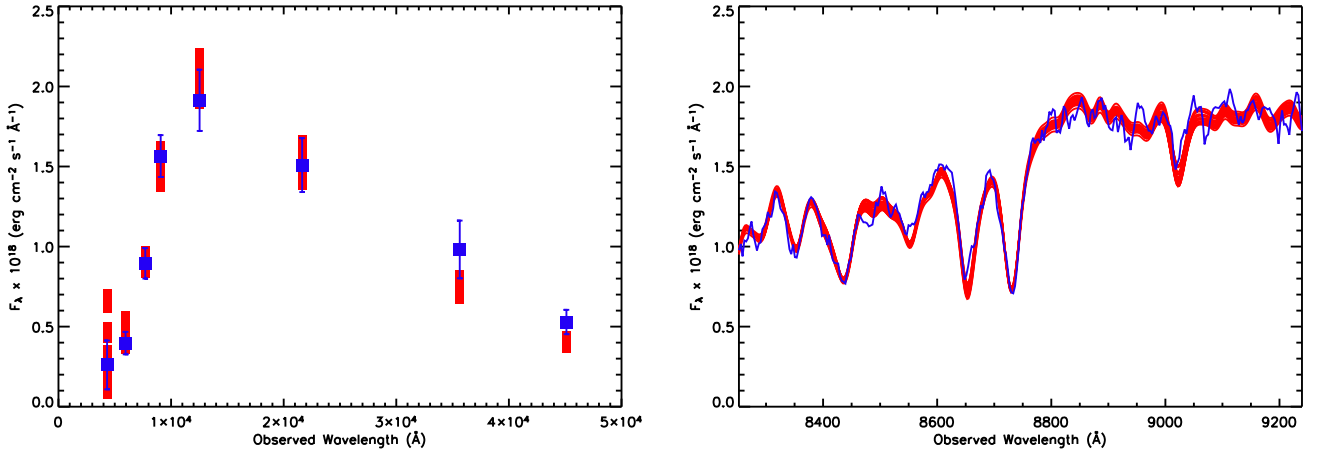


Fig. 3. Results from the fit of the GOODS spectrophotometric data with a delayed exponential SFH without secondary burst. *Left panel:* averaged observed (*blue* data points) and model SEDs (*red*); *Right panel:* stacked observed spectrum (*blue*) and models within 3σ confidence intervals.

The model spectra are smoothed to match the resolution of the GOODS and RDCS 1252 samples and cropped to a 500 Å interval centered on the 4000 Å break, which roughly corresponds to the high S/N, well flux-calibrated part of the spectra in our sample. This region also covers absorption features characteristic of young (e.g. H_δ) and old (e.g. CaII H&K) stellar populations. It includes the 4000 Å break, a good age indicator with mild metallicity sensitivity (e.g. Poggianti & Barbaro 1997), and therefore removes part of the degeneracy inherent to our grid of star formation histories. By using this relatively narrow wavelength interval, possible distortions due to uncertain flux calibration on the red end of the spectra (Demarco et al. 2007) are also minimized.

The BC03 models offer the choice of two initial mass functions (IMFs), Salpeter or Chabrier (2003). The choice of the IMF has little effect on the shape of the composite spectrum for the considered age range ($t \leq 5$ Gyr), as the Salpeter and Chabrier IMFs are nearly identical above $1 M_\odot$. We assume a Salpeter IMF for consistency with the photometric masses described in the previous section. The lower and upper mass cut offs are 0.1 and $100 M_\odot$ respectively (Bruzual & Charlot 2003).

Photometric errors are described in Rettura et al. (2006). Spectroscopic errors are based on the evaluation of the signal-to-noise ratio at 4100 Å rest-frame from the residuals after fitting the H_δ absorption line of the co-added spectra. The total response of the detector is then normalized to this value to obtain a noise estimate as a function of wavelength.

The stacked spectrum of the GOODS sample has a S/N of approximately 44 and an equivalent exposure time of $t_{exp} = 93h$. For the RDCS 1252 sample, the corresponding values are S/N \sim 20 and $t_{exp} = 74h$.

4. Results

To characterize the star formation history of the best fit models in our field and cluster samples, we define the final formation time t_{fin} of a given model as the time, after the onset of star formation, at which 99% of the final stellar mass has been formed. The corresponding look-back time since $z = 1.24$ to the final formation redshift z_{fin} is $T - t_{fin}$.

In Fig. 4, left panel, we plot the distribution of the difference between the age and final formation time, $T - t_{fin}$, of the best fit models which lie within the intersection of 3σ confidence levels of the photometric and spectral data for our field and cluster samples. The top axis gives the corresponding final formation redshift. We find that the mean final formation time of the cluster early-type galaxy population is ~ 1 Gyr greater than the corresponding population in the field, namely that field early-types have longer star formation time scales. We also note that the star-formation weighted ages of the two populations, as defined in Menci et al. (2008) and Rettura et al. (2008), differ by only ~ 0.5 Gyr on average, as shown in Fig. 5. This age difference is in very good agreement with that derived by van Dokkum & van der Marel (2007) from the evolution of the mass-to-light ratio, which is based on a completely independent method and data set. In Fig. 4, right panel, we plot the distribution of $T - t_{fin}$ of the models that lie within the 3σ confidence level from the photometric data only. We see that fitting only the stacked SEDs of our cluster and field sample yields very similar results and that the spectroscopic data carries most of the weight for the difference in final formation times. This can be appreciated in Fig. 6, where we divide our samples equally in two mass bins and show that the averaged spectrum of the cluster galaxies has a more pronounced 4000 Å break than that of the field sample, specifically at lower masses. This elucidates how the time scale of the star formation activity in the cluster environment is shorter than in the field, and such a difference becomes negligible for the most massive galaxies.

In Fig. 7, we plot the median stellar mass fraction, $m_\star(t)$, formed at time t after the onset of star formation in cluster and field galaxies. This is computed as the median of the integrated star formation rate (eq.1) of all models within the 3σ confidence levels. The error bars represent the standard deviation of the distribution of $m_\star(t)$. This difference

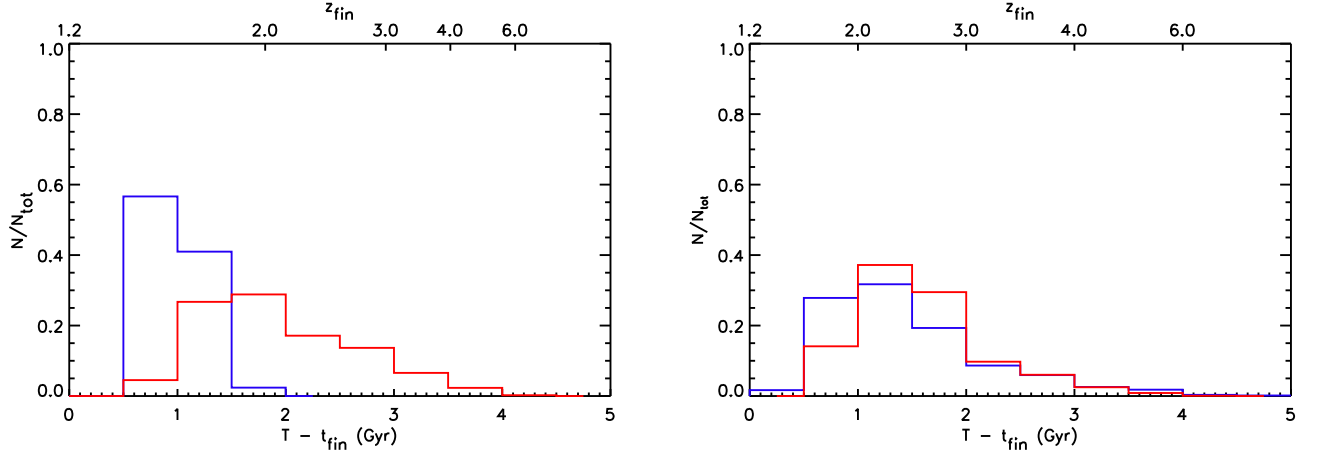


Fig. 4. Fraction of best fit models to the spectrophotometric (*left panel*) and photometric only (*right panel*) data, within the 3σ contours, as a function of final formation redshift z_{fin} and look-back time since $z = 1.23$, $T - t_{fin}$. The blue histogram corresponds to the GOODS field sample and the red one to the RDCS 1252 cluster sample.

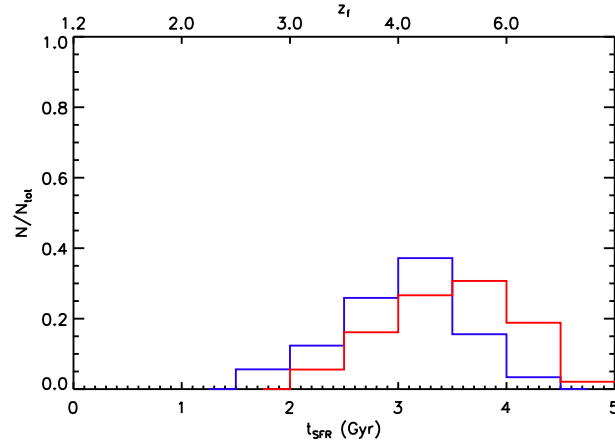


Fig. 5. Fraction of best fit models for the field (*blue*) and cluster (*red*) samples, as in Fig. 4, as a function of the star-formation weighted age $t_{SFR} = \int_0^T dt' (T - t') \Psi(t') / \int_0^T dt' \Psi(t')$.

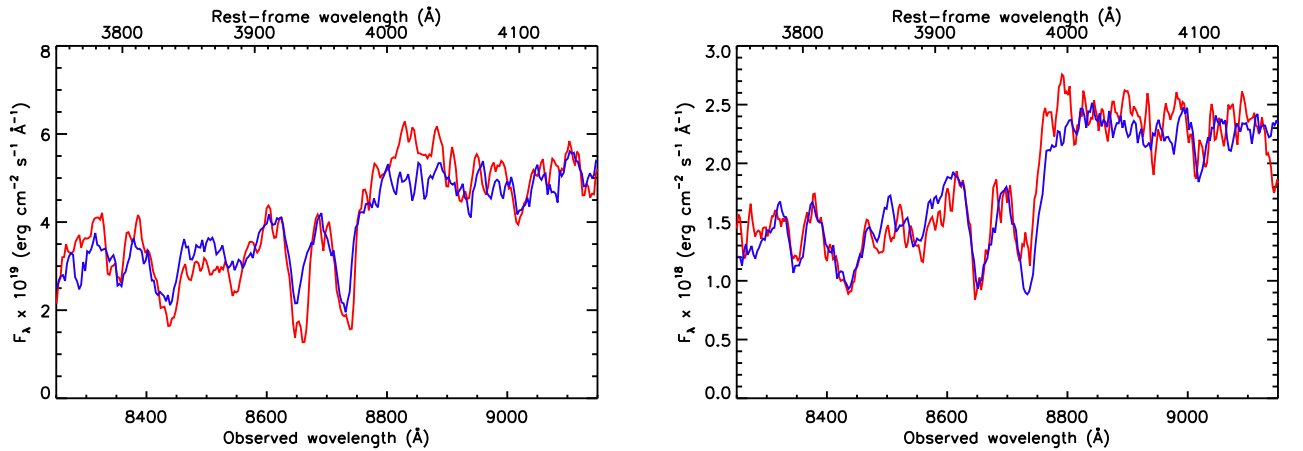


Fig. 6. Stacked spectra of low-mass ($M_* < 1.2 \times 10^{11} M_\odot$, *left panel*) and high-mass ($M_* \geq 1.2 \times 10^{11} M_\odot$, *right panel*) galaxies in the field (*blue*) and cluster (*red*) samples. The signal-to-noise ratios and equivalent exposure times are: 23, 47h (GOODS) and 17, 39h (RDCS 1252) for the low-mass bin (*left*); 42, 46h (GOODS) and 13, 36h (RDCS 1252) for the high-mass bin (*right*).

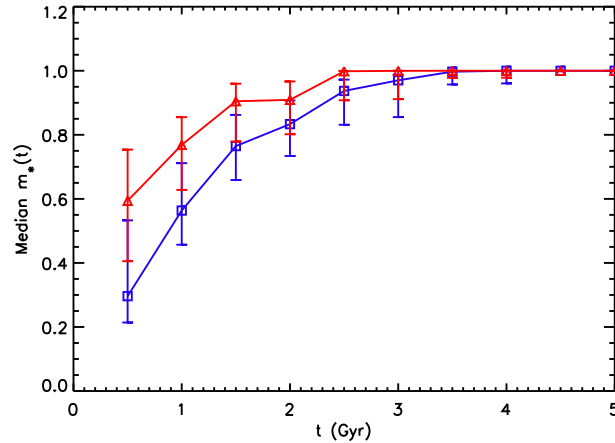


Fig. 7. Median stellar mass fraction of the best fit models as a function of the time since the onset of star formation, for the GOODS (*blue*) and RDCS 1252 (*red*) samples.

between the star formation histories of our cluster and field sample is even greater if we consider only the simple delayed exponential models.

To assess the constraining power of the spectrophotometric fit when using low signal-to-noise spectra, we perform a large set of Monte-Carlo simulations. We first use the BC03 model corresponding to the best fit parameters of the stacked spectrophotometry for each sample; for the GOODS sample we find $\{T = 4.25 \text{ Gyr}, \tau = 0.6 \text{ Gyr}, t_{burst} = 1 \text{ Gyr}, A = 0.5\}$, for RDCS 1252 $\{T = 5 \text{ Gyr}, \tau = 0.5 \text{ Gyr}, t_{burst} = 3 \text{ Gyr}, A = 0.2\}$. We add to the model SED (obtained by integrating the model spectrum over the filter curves) and spectrum an amount of noise consistent with that of our individual galaxies. We find that the region of parameter space occupied by the models that best fit the input spectrum overlaps completely with confidence levels of the fit of the input SED. Therefore, such low signal-to-noise spectra do not add more constraints on the star formation history than those given by the broad-band photometry alone. This confirms the need to co-add the spectrophotometric data.

We then investigate possible biases in our fitting approach with two different sets of simulations. First, each model spectrum in the $\{T, \tau, t_{burst}, A\}$ grid is redshifted to the observed frame and synthetic magnitudes are computed for our broad-band filters, assuming errors similar to those of our stacked spectrophotometric data. The resulting SED and spectrum is fitted using the approach described above. We then compare the parameters of the best fitting models with those of the input model. Because of the known degeneracy between age and τ (e.g., Gavazzi et al. 2002), we do not consider them separately but rather use the T/τ ratio. We also compare the median final formation time $t_{fin,fit}$ of the best fit models within the intersection of the 3σ confidence levels (see Fig. 2) to the formation time $t_{fin,0}$ of the input model. The distribution of $t_{fin,0} - t_{fin,fit}$ is found to be strongly peaked at 0 with a standard deviation of 0.5 Gyr. The distribution of $(T/\tau)_0 - (T/\tau)_{fit}$ likewise shows no bias (Fig. 8, left panel). We can therefore conclude that our fit reproduces reasonably well the original data and that any difference we find between our field and cluster samples is not an artifact of the method.

Secondly, we carry out a Monte-Carlo simulation on the single best fit model for the cluster and the field sample. We add to the model SEDs and spectra an amount of noise equal to that of our stacked spectrophotometric data and perform the χ^2 goodness-of-fit test described above. As shown in Fig. 8 (right panel), we do not find any appreciable differential bias between the two samples.

To determine whether the difference between our cluster and field samples is due to a selection effect, we also consider pairs of randomized samples constructed from both field and cluster galaxies. We first convert the b_{435} , v_{606} and J magnitudes of the GOODS sample to B, V and J_s , as used in RDCS 1252. We integrate the spectra of our grid of models to derive the photometric transformations at $z \simeq 1.2$:

$$B = b_{435} - 0.021 \times (b_{435} - v_{606}) + 0.0014 \quad (2)$$

$$V = v_{606} + 0.32 \times (b_{435} - v_{606}) + 0.081 \quad (3)$$

$$J_s = J - 0.03 \times (J - K_s) + 0.013 \quad (4)$$

In this test, we ignore the R band data of RDCS 1252 as there is no comparable band in the GOODS photometry. We construct one hundred sample pairs by drawing 21 galaxies randomly from GOODS and RDCS 1252 to constitute the 'cluster' sample and assigning the rest to the 'field' sample. We then perform the same fitting procedure, as described in Section 3, on these two separate pseudo-samples. As a measure of the difference between the two pseudo-populations, we consider the absolute difference in mean final formation times $\Delta < t_{fin} >$.

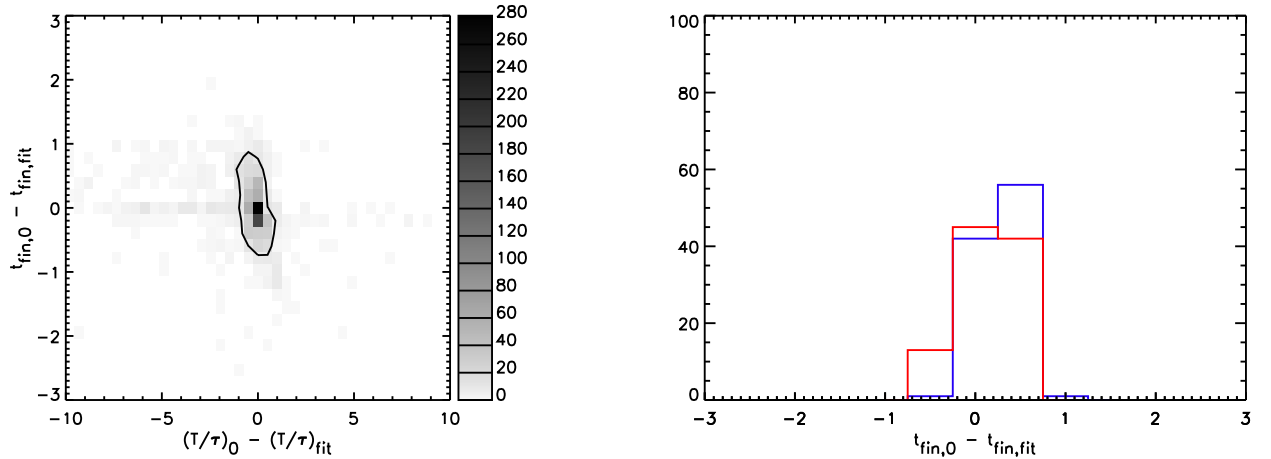


Fig. 8. *Left panel:* distribution of the difference between the input and best fit solution over the grid of models $\{T, \tau, t_{burst}, A\}$ for two relevant parameters: the formation time t_{fin} and the age/ τ ratio. The gray scale refers to the number of models in the grid. *Right panel:* distribution of the residuals of final formation times obtained by perturbing the best fit model of the GOODS (*blue*) and RDCS 1252 (*red*) samples.

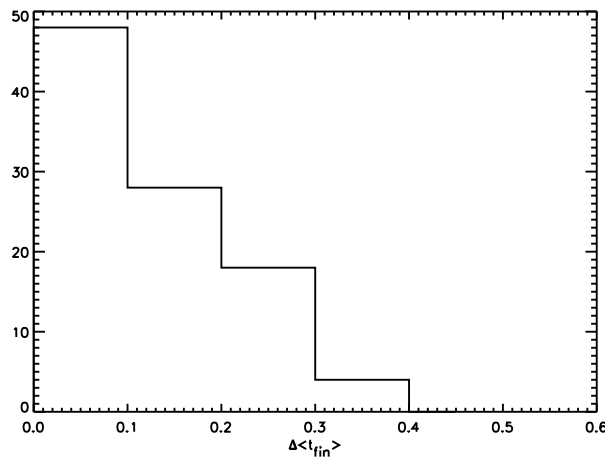


Fig. 9. Distribution of the difference between the mean formation times of 100 pairs of randomized samples.

Fig. 9 shows the distribution of $\Delta \langle t_{fin} \rangle$ in our pseudo-cluster and field sample pairs. We see that it is peaked at $\Delta \langle t_{fin} \rangle = 0$ and that the value of ~ 1 Gyr derived from the GOODS and RDCS 1252 samples lies well outside this distribution. This implies that the galaxies in our field and cluster samples are drawn from two distinct populations.

We stress that our field sample is more deficient in lower mass galaxies with respect to the total photometric sample than our cluster sample (see Fig. 1). This however does not affect our conclusions. Even if the field sample were corrected for completeness, the averaged SED and spectrum would be expected to appear bluer and thus younger, amplifying the difference between the star formation histories of the field and the cluster. As widely reported in the literature, we also find that less massive galaxies are best fitted with younger stellar population models (the so-called “downsizing”). Unfortunately, we do not have enough statistics to study whether at this redshift the mass-age correlation varies from cluster to field.

Since age and metallicity have a similar effect on the spectrum of a stellar population, the difference we observe between our field and cluster samples might not correspond to distinct star formation histories, but to a difference in metal content. To quantify this effect, we compare our average field galaxy data to sub-solar metallicity models computed using the GALAXEV code and the same grid of parameters as before, keeping the cluster galaxies at solar metallicity.

As shown in Fig. 10, the star formation histories of our cluster and field samples coincide if one population is assumed to be approximately a factor of five more metal rich than the other. However, this ad hoc assumption does not appear to be realistic. At low redshift, the variation in metallicity of early type galaxies with environment was found to be less than 0.1 dex (Thomas, Maraston & Bender 2005), with field ellipticals being more metal-rich than their cluster counterparts. As the bulk of star formation in cluster and field ellipticals is understood to have occurred at $z > 2$ (Renzini 2006), it is unlikely that the relative metallicity of field and cluster ellipticals is different at these redshifts.

As with metallicity, age and dust content are largely degenerate when fitting SEDs. However, since we use high-resolution spectra as well as SEDs, our method is less sensitive to dust than to metallicity. In this work, extinction by

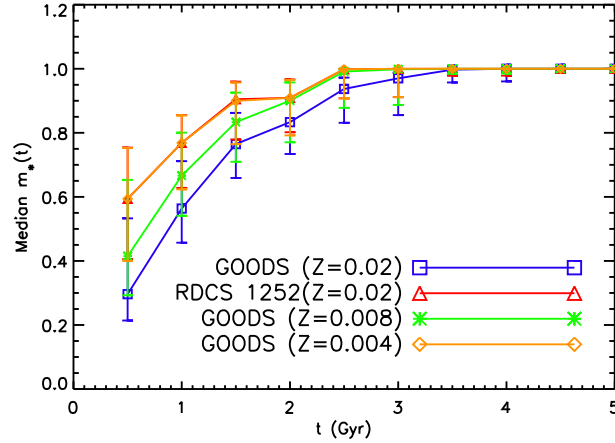


Fig. 10. Median stellar mass fraction of the best fit models as a function of the time since the onset of star formation, for RDCS 1252 at solar metallicity and GOODS at solar and sub-solar ($[Z/H]=0.008, 0.004$) metallicities.

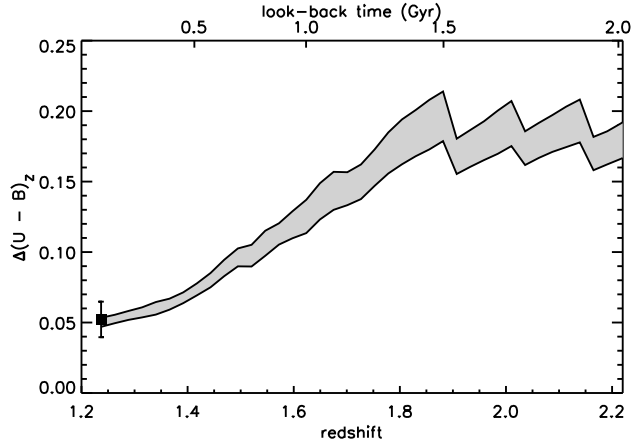


Fig. 11. Predicted rest-frame $(U - B)_z$ scatter of the red sequence of RDCS 1252 extrapolated to $z = 2.2$. The shaded area represents the rms dispersion of the models that best fit the SEDs of all red sequence galaxies. The filled square is derived from the $i_{775} - z_{850}$ scatter measured by Blakeslee et al. (2003).

dust is not taken into account, as Rettura et al. (2006) found that the SEDs of RDCS 1252.9-2927 member galaxies are best fitted by models with no or little dust extinction. Furthermore, there is no evidence that dust structures in early type galaxies contribute significantly to their mid-IR spectrum (Temi et al. 2005) or are correlated with environment (Tran et al. 2001).

We also measure the synthetic scatter of the rest-frame $(U - B)_z$ color, $\Delta(U - B)_z$, of the early-type (E and S0) galaxies lying on the red sequence of RDCS 1252 using the morphological classification and selection criterion described by Blakeslee et al. (2003), for galaxies brighter than $z_{850} = 24.0$ (this yields 33 red sequence galaxies). Rest frame $(U - B)_z$ colors are obtained for each galaxy using the model that best fits the 9-band SED. For this purpose, we use only simple delayed, exponentially declining star formation histories parametrized by T and τ (see Section 3). We find good agreement with the Blakeslee et al. measurement (0.05 mag intrinsic scatter). We can then use these models to predict the evolution of the $(U - B)_z$ scatter with redshift and corresponding look-back time from $z = 1.24$ up to $z = 2.2$. At each redshift, the scatter is measured applying a 3σ clipping around the linear best fit, as customary in the literature. A few additional galaxies drop out of the red sequence sample as the redshift becomes larger than their formation redshift. We estimate the uncertainty on the scatter at each redshift by randomly perturbing the SED of each galaxy, assuming Gaussian errors on the fluxes. Fig. 11 shows that the red sequence dissipates at $z \sim 1.9$, reaching scatter values comparable with those observed in the red population of the field up to $z \sim 2$ (Cassata et al. 2008). At $z \sim 1.9$, 25 galaxies out of the original 33 are still included in the red sequence sample. This redshift is also consistent with the median final formation redshift derived from the analysis of the stacked spectrophotometric data. A similar analysis using $(U - V)_z$ and $(U - R)_z$ scatters yields the same result. We can conclude that the red sequence in such a massive cluster is established in ~ 1 Gyr, and it is therefore not surprising that recent analysis of forming red sequences in protoclusters at $z > 2$ find a significant scatter (Kodama et al. 2007, Tanaka et al. 2007, Zirm et al. 2007).

5. Conclusion

We compared the underlying stellar population properties of $z \simeq 1.2$ early-type galaxies in the very high density environment of the massive cluster RDCS 1252 with those in the GOODS field. We derived star formation histories by fitting both the spectroscopic and the broad band photometric data with a large grid of stellar population synthesis models. To this purpose, we select 43 early-type galaxies (21 in the field and 22 in the cluster) all with stellar masses greater than $M_{lim} = 5 \times 10^{10} M_{\odot}$, $i_{775} - z_{850} \geq 0.8$ and the absence of the [OII] $\lambda 3727$ line in the spectra. These criteria naturally select all galaxies on the red sequence of RDCS 1252. For each sample, we use the co-added spectrophotometric data of the galaxies and compare them with BC03 models of exponentially declining star formation rates with an additional burst.

We find a small although significant difference in the star formation histories of the cluster and field populations, suggesting that the cluster galaxies form the bulk of their stars ~ 0.5 Gyr earlier than their counterparts in the field, with massive early-type galaxies having already finished forming stars at $z > 1.5$ in both environments. This difference is particularly evident at masses $\lesssim 10^{11} M_{\odot}$, which are characterized by a longer star formation time scale, resulting in a final formation time delayed by ~ 1 Gyr, whereas it becomes negligible for the most massive galaxies. While our differential analysis of the stellar population parameters of cluster and field galaxies in the same mass range convincingly shows distinct star formation histories, the absolute age difference remains model dependent. In an accompanying paper, Rettura et al. (2008) have analyzed the rest-frame far-UV flux of the same sample of early-type galaxies and found that field galaxies are at least 0.5 mag brighter than the RDCS 1252 galaxies in the same mass range. Our best fit models consistently predict this magnitude difference, which is indicative of the longer star formation time scale of the field galaxies. We have verified that such a difference in derived star formation histories in the two environments cannot be ascribed to incompleteness of the mass selected samples, which would tend to rather increase such an effect. We also used extensive Monte-Carlo simulations to identify possible biases in the model fit, and discussed the effect of inherent degeneracies such as metallicity and dust. We note that independent studies of massive early-type galaxies based on the measurement of the mass-to-light ratios of massive early-type galaxies in high- and low-density environments (Treu et al. 2005, van der Wel et al. 2005, van Dokkum & van der Marel 2007) have reached similar conclusions.

We also used the best fit star formation histories from the 9-band SEDs of the red sequence galaxies in RDCS 1252 to predict that a tight ($\Delta(U - B)_z = 0.05$ mag) red sequence at $z = 1.2$ is established over approximately 1 Gyr and dissolves by $z \approx 1.9$. This suggests that for massive clusters, which have long reached virialization by redshift 1.2, we do not expect a significant red sequence at $z > 2$, i.e. a $(U - B)_z$ color scatter well above 0.1 mag.

These observations and analysis can be used to provide significant constraints on galaxy evolution models in a hierarchical scenario (e.g. Menci et al. 2008), which predicts the evolution in high-density environments to be accelerated compared to the field.

Acknowledgements. This research was partially supported by the DFG cluster of excellence “Origin and Structure of the Universe” (www.universe-cluster.de)

References

- Blakeslee, J.P., Franx, M., Postman, et al. 2003, ApJ, 596, L143
- Bruzual, G., Charlot, S. 2003, MNRAS, 344, 1000
- Benítez, N. 2000, ApJ, 536, 571
- Bernardi, M., Renzini, A., Da Costa, L.N. et al. 1998, ApJ, 507, L43
- Cassata, P., Cimatti, A., Kurk, J. et al. 2008, A&A, 483, 39
- Clemens, M.S., Bressan, A., Nikolic, B. et al. 2006, MNRAS, 370, 702
- Coleman, G.D., Wu, C.-C., Weedman, D.W. 1980, ApJS, 43, 393
- De Lucia, G., Springel, V., White, S.D.M., Kauffmann, G. 2006, MNRAS, 366, 499
- Demarco, R., Rosati, P., Lidman, C. et al. 2007, ApJ, 663, 164D
- di Serego Alighieri, S., Lanzoni, B., Jørgensen, I. 2006, ApJ, 647, L99
- Eggen, O.J., Lynden-Bell, D., Sandage, A.R. 1962, ApJ, 136, 748
- Gavazzi, G., Pierini, D., Boselli, A. 1996, A&A, 312, 397
- Gavazzi, G., Bonfanti, C., Sanvito, G., Boselli, A., Scodreggio, M. 2002, ApJ, 576, 135
- Giavalisco, M., Ferguson, H.C., Koekemoer, A.M. et al. 2004, ApJ, 600, 93
- Häussler, B., McIntosh, D.H., Barden, M. et al. 2007, ApJS, 172, 615
- Kodama, T., Tanaka, I., Kajisawa, M. et al. 2007, MNRAS, 377, 1717
- Lidman, C., Rosati, P., Demarco, R. et al. 2004, A&A, 416, 829
- Menci, N., Rosati, P., Gobat, R. et al. 2008, ApJ, in press
- Oke, J.B. 1974, ApJS, 27, 21
- Poggianti, B.M., Barbaro, G. 1997, A&A, 325, 1025
- Renzini, A. 2006, ARA&A, 44, 141
- Rettura, A., Rosati, P., Strazzullo, V. et al. 2006, A&A, 458, 717
- Rettura et al., 2008, submitted to ApJ
- Rosati, P., Tozzi, P., Ettori, S. et al. 2004, ApJ, 127, 230
- Salpeter, E.E. 1955, ApJ, 121, 161
- Sánchez-Blázquez, P., Gorgas, J., Cardiel, N., González, J.J. 2006, A&A, 457, 809
- Sandage, A. 1986, A&A, 161, 89
- Strazzullo, V., Rosati, P., Stanford, S.A. et al. 2006, A&A, 450, 909
- Tanaka, M., Tadayuki, K., Kajisawa et al. 2007, MNRAS, 377, 1206
- Tem, P., Brighenti, F., Mathews, W.G. 2005, ApJ, 635, L25
- Thomas, D., Maraston, C., Bender, R., Mendes de Oliveira, C. 2005, ApJ, 621, 673

- Toft, S., Mainieri, V., Rosati, P. et al. 2004, A&A, 422, 29
- Toomre, A. 1977, In *Evolution of Galaxies and Stellar Populations*, ed. BM Tinsley & RB Larson, New Haven:Yale University Observatory, p. 401
- Tran, H.D., Tsvetanov, Z., Ford, H.C., Davies, J. 2001, ApJ, 121, 2928
- Treu, T., Ellis, R.S., Liao, T.X., van Dokkum, P.G. 2005, ApJ, 622, 5
- van der Wel, A., Franx, M., van Dokkum, P.G., Rix, H.-W., Illingworth, G.D., Rosati, P. 2005, ApJ, 631, 145
- van Dokkum, P.G., Franx, M., Kelson, D.D., Illingworth, G.D. 2001, ApJ, 553, L39
- van Dokkum, P.G., van der Marel, R.P. 2007, ApJ, 655, 30
- Vanzella, E., Cristiani, S., Dickinson, M. et al. 2006, A&A, 454, 423
- Vanzella, E., Cristiani, S., Dickinson, M. et al. 2008, A&A, 478, 83
- Zirm et al. 2008, ApJ, 680, 224